XL CILAMCE
IBERO-LATIN AMERICAN CONGRESS ON COMPUTATIONAL METHODS IN ENGINEERING
NOVEMBER 11-14, 2019
Praiamar Natal Hotel & Convention Natal, RN-BRAZIL

THE EFFECT OF FRACTURE TREATMENT PARAMETERS ON DIAGNOSTIC FRACTURE INJECTION TESTS (DFIT)

Renan Marks de Oliveira Pereira
Eleazar Cristian Mejia Sanchez
Deane Roehl
renanmarks@tecgraf.puc-rio.br
crisms@tecgraf.puc-rio.br
deane@tecgraf.puc-rio.br
Tecgraf Institute and Civil and Environmental Engineering Department, PUC-Rio
Rua Marques de São Vicente, 225, Gávea, 22453900, Rio de Janeiro, RJ, Brasil

Abstract. In-situ stresses and permeability of the rock media has a significant role in predicting the production rate of oil and gas reservoirs. Hydraulic fracturing is a widely used technique to increase the rock formation permeability in oil and gas reservoirs. The diagnostic fracture injection test (DFIT) is a commonly used and reliable technique executed prior to a hydraulic fracture stimulation process. Its main objective is to break a small fracture in the rock formation around the wellbore, in order to evaluate the closure of the fracture system. This test provides the parameters necessary for hydraulic fracturing planning, such as minimum horizontal stress, fracture closure pressure, fracture gradient, fluid leak-off coefficient, fluid efficiency, and formation permeability. These parameters play an important role in determining the operation window for stability and planning of secondary recovery operations. This work presents the numerical simulation of a DFIT in a carbonate reservoir of a Brazilian oil field. Coupled hydro-mechanical continuum elements and coupled cohesive interface elements represent the porous media and the hydraulic fracture in the numerical model, respectively. This paper aims at investigating the effect of fracture treatment parameters on the hydraulic fracture geometry before- and after-closure response of the DFIT. The methodology reproduces numerically all stages of a DFIT. Therefore, the comparison of the measured bottom-hole pressure and those obtained numerically show good agreement. The right combination of minimum in-situ stress and permeability estimation was essential to obtain a good closure response after shut-in.

Keywords: Diagnostic Fracture Injection Test (DFIT); Permeability; Hydraulic fracture; Closure stress

1 Introduction

Brazilian Pre-Salt carbonates are a deep set of reservoirs located below a thick layer of salt, in deep water depths and occupy an area of 160,000 km². The Pre-Salt layer spreads throughout the Santos, Campos and Espírito Santo Basins, from the coast of the Santa Catarina State to the coast of Espírito Santo State [1]. These carbonates are characterized by a low to medium porosity (15-25%) and low permeability (1-10mD). The carbonate reservoirs are situated in water depths close to 2200m and reservoir depths reach up to 7000m [2]. Despite the challenges, due to very low permeability of reservoirs, stimulation is required in order to enhance reservoir productivity.

Diagnostic Fracture Injection Tests (DFIT), which is also referred as Injectivity Tests, Step Rate Tests, and Mini-Frac Tests, have been used in the last few decades as the most reliable technique to predict the in-situ stresses [3]. These techniques are commonly executed prior to a reservoir stimulation process. During a DFIT, a small volume of water is injected into the reservoir at a low injection rate for a few minutes in order to create fractures which propagate through the formation. In the shut-in period, which comes after the injection process, the pressure is also monitored. The resulting wellbore pressure provides an estimation of reservoir properties, such as the in-situ stresses, the breakdown pressure, the fracture propagation pressure, the closure pressure, and the permeability of the reservoir [4–6].

Fracture initiation and propagation in continuum solids require the use of a criterion to predict and control when the fracture should grow. The cohesive zone model (CZM) contrasts with the conventional fracture mechanics which is based on infinitely sharp fracture models. When the aperture of the CZM law reaches a critical value at which the cohesive traction disappears, the CZM approach cancels the stress singularity at the crack tip [7–10]. This method is a powerful and efficient technique for computational fracture modeling. Complex problems such as hydraulic fracturing and even the interaction between the hydraulic and natural fractures are eligible for modelling with CZM [11,12]. Other techniques are found in literature for modelling fractures as well [13–15]

This work aims at discussing the effect of the parameters necessary for a numerical simulation of a DFIT. The field-measured data of DFIT executed in the Espírito Santo Basin is extracted from the paper of Azevedo *et al*. [2]. The problem is studied using coupled hydro-mechanical continuum elements and coupled cohesive interface elements to represent the porous media and the hydraulic fracture in the numerical model, respectively. The effect of some initial field conditions such as in situ stresses, permeability and fracture height is also studied. Good agreement is found between the Bottom-Hole pressures obtained from the numerical analysis and the values measured in the field.

2 Governing Equations

The physical process of the fluid-driven fracture involves the pumping of a fracturing fluid that pressurizes the fracture surfaces, leading to the rock hydraulic fracturing. In this process, there is a strong coupling between the rock deformation, the moving fluid (in porous media and in the fracture) and fracture propagation.

The governing equations for these hydro-mechanical coupled processes includes Biot's theory of poroelasticity for porous media, Darcy's law for pore fluid flow, Reynold's lubrification theory for fracturing fluid flow, and Cohesive Zone model to represent the fracture behavior.

2.1 Rock Deformation

In 1941, the basic theory of poroelasticity was introduced by Biot [16], which was originally developed for consolidation problems. Since then, many researchers have contributed to its development, and in 1976, Rice and Cleary [17] reformulated the theory in a more physically relevant manner to account for the poroelastic effects.

A poroelastic system requires five material constants including the drained shear modulus G, the drained Poisson ratio ν, the undrained Poisson ratio ν_u, the Skempton's pore pressure coefficient B, and

the intrinsic permeability κ. For soil or rock type material, these constants can be associated to micromechanical parameters [17] : porosity n, fluid bulk modulus K_f, solid grain bulk modulus K_s, porous bulk modulus for the solid skeleton K, Poisson's ratio ν, and permeability κ.

The equilibrium equation with poroelastic constitutive relation, assuming small strains is given by

$$\sigma_{ij} - \sigma_{ij}^0 = 2G\varepsilon_{ij} + \left(K - \frac{2}{3}G\right)\varepsilon_{kk} - \alpha(p - p_0)\delta_{ij} \tag{1}$$

The total stresses σ_{ij} are related to Terzaghi's effective stresses σ'_{ij} through

$$\sigma_{ij} = \sigma'_{ij} + \alpha p \tag{2}$$

where α is Biot's coefficient, which is independent of the fluid properties, and it is defined as

$$\alpha = \frac{3(\nu_u - \nu)}{B(1 - 2\nu)(1 + \nu_u)} = 1 - \frac{K}{K_s} \tag{3}$$

It is important to notice that α is necessary when applying this formulation to rock materials, in order to consider the compressibility of the constitutive materials. The constitutive relation in terms of effective stress and strains are simplified as

$$\alpha\sigma'_{ij} - \sigma'^0_{ij} = 2G\varepsilon'_{ij} + \left(K - \frac{2}{3}G\right)\varepsilon'_{kk}\delta_{ij} \tag{4}$$

The problem states the effective stress principle for porous media, with its solution limited to a bi-dimensional formulation. Numerical approximation of the poroelasticity theory can follow with the finite element method (FEM) and a standard Galerkin formulation [18,19]. The FEM equations for the equilibrium and continuity equation are as follows:

$$[K]\{u\} + [L]\{p\} = \{F\} \tag{5}$$

$$[S]\{\dot{p}\} + [L]^T\{\dot{u}\} + [H]\{p\} = \{q\} \tag{6}$$

where u are the nodal displacements, p are the nodal pressures, F are the nodal forces q are the nodal flows, $[K]$ is the stiffness matrix, $[L]$ is the coupling matrix, $[H]$ is the flow matrix, and $[S]$ is the compressibility matrix. In a discretized form, the unknown field parameters u and p are expressed by the nodal values, and the interpolation functions enter in the calculation of the matrices as

$$p = N^p\{p\}, \quad u = N^u\{u\}, \quad \varepsilon = \mathrm{B}\{u\} \tag{7}$$

where N^p and N^u are the nodal shape functions for pressure and displacements, respectively. B is the strain-displacement matrix. The matrices in the system of Eqs. (5) and (6) are given by the following expressions:

$$[K] = \int_{\Omega} B^T D B d\Omega, \qquad [L] = \alpha \int_{\Omega} N^u \begin{Bmatrix} \frac{d}{dx} \\ \frac{d}{dy} \end{Bmatrix} N^p d\Omega$$
$$[S] = \int_{\Omega} (N^p) \frac{1}{M} N^p \, d\Omega, \quad [H] = \kappa \int_{\Omega} N^u \begin{Bmatrix} \frac{d}{dx} \\ \frac{d}{dy} \end{Bmatrix}^T N^p \begin{pmatrix} \frac{d}{dx} \\ \frac{d}{dy} \end{pmatrix} N^p d\Omega \tag{8}$$

where D is the elasticity constitutive matrix for drained material.

2.2 Pore Fluid flow

Assuming small volumetric grains, the continuity equation for the pore fluid is given by

$$\frac{1}{M}\dot{p} + \alpha \dot{\varepsilon}_{kk} + v_{k,k} = 0 \tag{9}$$

where v_k is the pore fluid velocity, and M is the Biot's modulus.

$$\frac{1}{M} = \frac{\phi_0}{K_f} + \frac{\alpha - \phi_0}{K_S} \tag{10}$$

ϕ_0 is the initial porosity. Pore fluid is assumed to flow through an interconnected pore network according to Darcy's law

$$v_i = -\frac{k}{\mu_m} p_{,i} = -\frac{\bar{k}}{\gamma} p_{,i} \tag{11}$$

in which k is the permeability, μ_m is the pore fluid viscosity, $\bar{k}$ is the hydraulic conductivity and γ is the pore fluid specific weight. Combining with the continuity equation, the pore fluid diffusion equation is

$$\frac{1}{M}\dot{p} + \alpha \dot{\varepsilon}_{kk} = \frac{\bar{k}}{\gamma} p_{,i} \tag{12}$$

2.3 Fracturing Fluid Flow

The fluid flow inside the fracture follows the Reynold's lubrification theory, which assumes laminar flow of an incompressible uniformly viscous Newtonian fluid. The continuity equation of one-dimensional flow is

$$\dot{w} + \frac{\partial q_f}{\partial s} + v_T + v_B = 0 \tag{13}$$

where q_f is the longitudinal flow rate along the fracture in s -direction, w is the crack opening and v_T

and v_B are the normal flow velocities of fracturing fluid leaking through the top and bottom faces of fracture to the rock formation.

Deriving the conservation of momentum balance for incompressible flow and considering a Newtonian fluid flow between parallel plates, the longitudinal flow rate is obtained

$$q_f = -\frac{w^3}{12\mu_f}\frac{\partial p_f}{\partial s} \tag{14}$$

where p_f denotes the fluid pressure on the fracture surface with the curvilinear coordinate s and μ_f is the dynamic fluid viscosity. Figure 1 shows the schematic representation of the fracturing fluid flow pattern within the fracture.

Eq. (14) determines the pressure profile along the fracture from the local aperture and the local flow rate. According to Eq. (14), the pressure gradient is very sensitive to fracture aperture. Therefore, a large pressure drop takes place within a small area near the crack tip where the aperture decreases substantially.

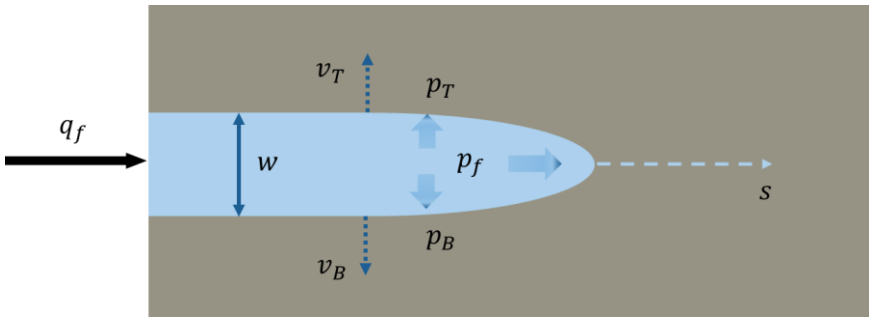

Figure 1 – Schematic representation of fracturing fluid flow pattern inside the fracture.

The normal fracturing fluid velocities are

$$\begin{aligned} v_T &= c_T(p_f - p_T) \\ v_B &= c_B(p_f - p_B) \end{aligned} \tag{15}$$

where c_T and c_B are the leak-off coefficients and p_T and p_B are the pore fluid pressures at the top and bottom faces of the fracture. Combining Eq. (13), (14) and (15) yields

$$\dot{w} + c_T(p_f - p_T) + c_B(p_f - p_B) = \frac{\partial}{\partial s}\left(\frac{w^3}{12\mu_f}\frac{\partial p_f}{\partial s}\right) \tag{16}$$

2.4 Cohesive Zone Model

The cohesive zone model (CZM) implies that normal stress continues to be transferred across a discontinuity as shown in Figure 2. The traction–separation relation of the CZM constitutive behavior comes from laboratory tests.

The fracture propagates after the normal stress falls to zero through a separation function. Fracture propagation is controlled by the energy balance between the work of the external loads and the sum of the bulk energy of the undamaged part and the energy dissipated in the fracture process. The CZM assumes that a narrow band is located in front of the fracture tip.

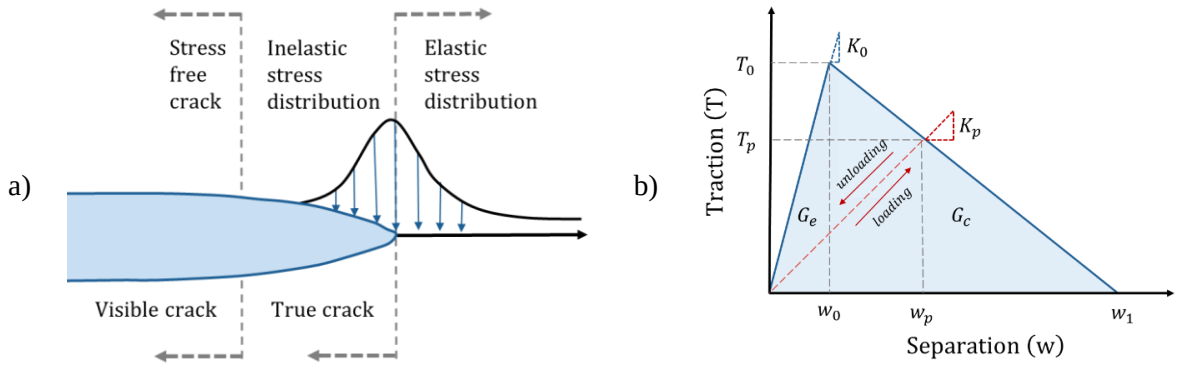

Figure 2 – a) Representation of the fracture process zone and b) The constitutive cohesive zone law

With increasing separation, the traction across the cohesive surface reaches a peak value T_0 and then decreases until zero, allowing a complete separation w_1.

Simple cohesive models can be described by two independent parameters which are usually, for mode I plane strain, the normal work of separation or the fracture energy G_C and either the tensile strength T_0 or the complete separation length w_1 [20,21]. An additional parameter in these models is the slope of the initial loading which may define a range from rigid-softening to elastic-softening response under tensile stress state.

As damage grows, the fracture is pressurized by the fracturing fluid pressure, p_f, calculated from the fracturing fluid equations Eq. (16). The total tractions resisted by the interface elements are therefore given by

$$T = K_p w - p_f \quad 0 \leq w \leq w_p \tag{17}$$

In this work, damage is assumed to initiate when the quadratic interaction function involving the stress ratios reaches a value of one, $f = 1$. The quadratic nominal stress criterion is

$$f = \left\{\frac{\langle t_n \rangle}{t_n^0}\right\}^2 + \left\{\frac{t_s}{t_s^0}\right\}^2 + \left\{\frac{t_t}{t_t^0}\right\}^2 \tag{18}$$

For the numerical implementation of the CZM, two-dimensional, isoparametric, 4-node or, 6-node interface elements are employed along the propagation direction.

3 DFIT Case

This work presents the numerical simulation of DFIT in a carbonate reservoir located in Espírito Santo Basin. Part of its Pre-Salt carbonate is characterized by a low permeability reservoir. Its fluid viscosity is approximately 0.70×10^{-3}Pa · s and the reservoir temperature is 130ºC. The top and bottom of the pay zone are 4310 and 4380 meters. The measured pore pressure at the top of the pay zone is 48 MPa [2].

3.1 Injectivity Test

The numerical calibration of DFIT consists of an injectivity test. A volume of 9.5 m³ (60 bbl) of completion fluid was pumped at a flow rate of 0.04 m³/s (14.6 bpm) into the well. Figure 3 shows the bottom-hole pressure (BHP) and the injection fluid rate measured during the test.

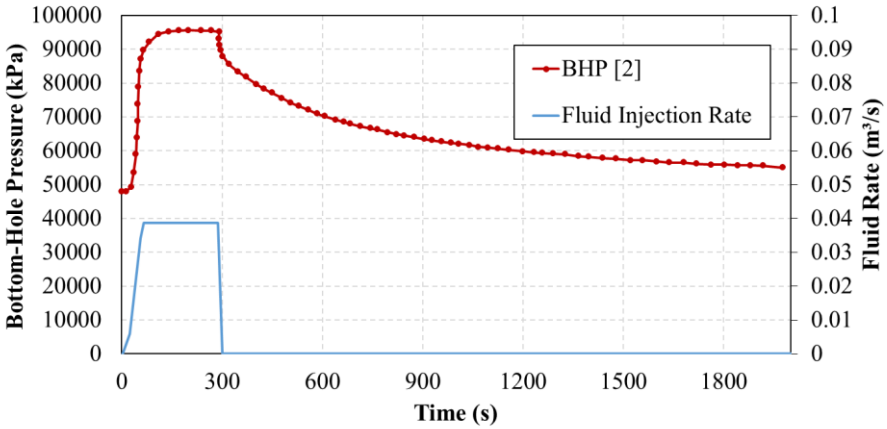

Figure 3 – The bottom-hole pressure and the fluid injection rate of an injectivity test[2]

3.2 Numerical model

The governing equations are discretized in space and time with the finite element method. Quadrilateral elements with full integration under plane strain conditions are used to approximate the displacement and pore pressure degrees of freedom of the porous media. While cohesive elements with two additional middle nodes of pore pressure are used to model the fluid flow within the fracture.

The injectivity test is executed in a deep carbonate reservoir in an interval from 4329 to 4359m. The two-dimensional numerical consists of a rectangular carbonate block of 600×450 m and a predefined fracture path at the middle (x=300m) along which the cohesive elements are inserted. The geometry and boundary conditions are shown in Figure 4.

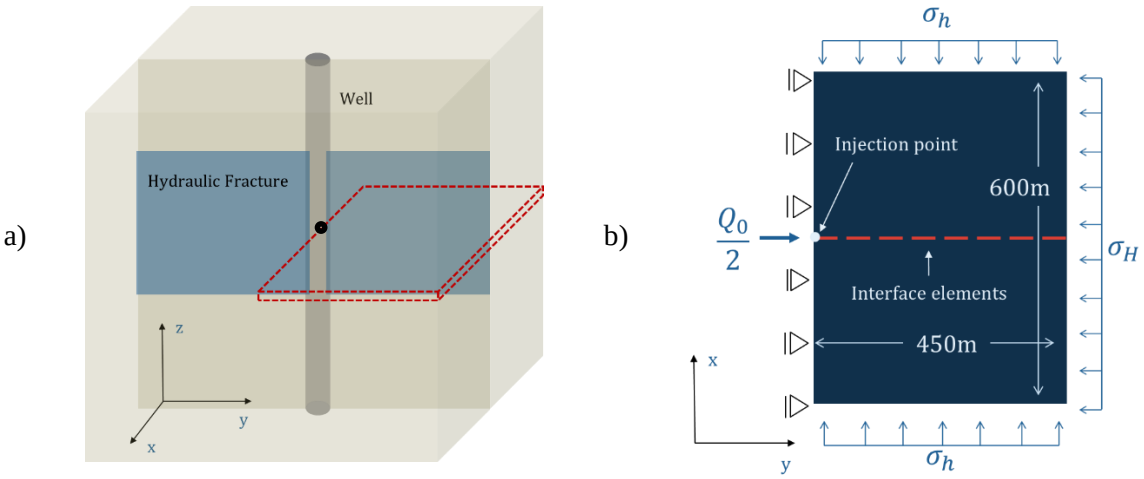

Figure 4 – Geometry and boundary conditions: a) Tridimensional and b) two-dimensional model.

The injection point is located in the middle of the left boundary, and the fracture is assumed to grow equally in both directions along the x-axis, which justifies the symmetry condition. Compared to the fracture length, the geometry of the wellbore is lower and neglected in the model. In all simulations, the hydraulic fracture propagates from an initial open fracture of 0.1 m in length.

In order to avoid sharp variations in the numerical results because of the fracture energy released during fracture propagation, a fine mesh is placed around the predefined fracture path to ensure numerical accuracy, as displayed in Figure 5.

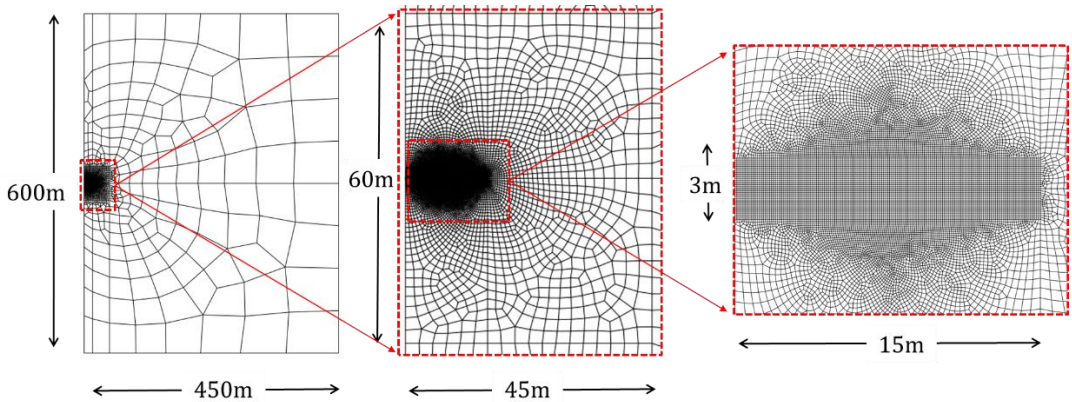

Figure 5 – Mesh refinement with 13165 elements

Before the hydraulic fracturing propagation process, the in-situ pore pressure and the stresses are initialized in the geostatic step in order to ensure the initial equilibrium state in the model. The minimum horizontal stress σ_h and the maximum horizontal stress σ_H are applied in the y- and x-directions respectively. For a kick start of the in-situ stresses, Equation (19) shows how the magnitude of σ_H is estimated in respect to the minimum horizontal stress σ_h [22].

$$\sigma H_{max} = \sigma h_{min} - P_b - P_p + T_0 \tag{19}$$

where P_b is the breakdown pressure, P_p is the poro pressure and T_0 is the tensile strength. The initial values of P_b, P_p and σh_{min} are estimated from the field-measured bottom-hole pressure curve.

For the hydraulic fracture modelling, the transient pressure response follows the following assumptions:

- The reservoir is isotropic and homogeneous and contains a compressible fluid.
- The fluid viscosity, formation porosity, and total compressibility are independent of pressure.
- Gravity effects are negligible
- Mechanically closed fracture has residual fracture aperture so it is still subject to leak-off and the fracture leak-off surface area remains unchanged.

4 Results and discussion

This section presents the numerical results including the effects of the in-situ stresses, permeability and fracture height parameters. Figure 3 exhibits the fluid injection rate considered in all simulations. Table 1 and Table 2 summarize the set of parameters adopted for the porous media and the hydraulic fracture in the numerical simulation of DFIT.

Table 1 – Input parameters

Parameter	Units	Value
Young modulus, E	kPa	45×10^6
Poisson ratio, ν	---	0.23
Biot's coefficient, α	---	0.95
Viscosity, μ_f	kPa s	7×10^{-7}
Injection rate, q	m³/s	0.04
Permeability, k	mD	1~10
Void ratio, ϕ	---	0.2
Pore pressure	kPa	48000

Table 2 – Cohesive zone model properties

Parameter	Units	Value
Tensile strength, T_0	kPa	3500
Fracture energy G_f	kPa.m	0.2
Loading stiffness, K_n	kPa	45×10^7

4.1 In-situ stresses effect

As the reservoir is characterized by permeability which ranges from 1 to 10 mili-Darcy, the effect of in-situ stresses is studied considering a permeability of 5 mili-Darcy for the porous media. Two different in situ stress scenarios, σ_h equal to 75 MPa and 85 MPa, are assumed. The maximum horizontal stress σ_H and the effective stresses are calculated as shown in the section 2. The numerical simulations are performed considering the material properties detailed in Table 1 and Table 2. Figure 6 shows the bottom-hole pressure during the simulation for these two scenarios.

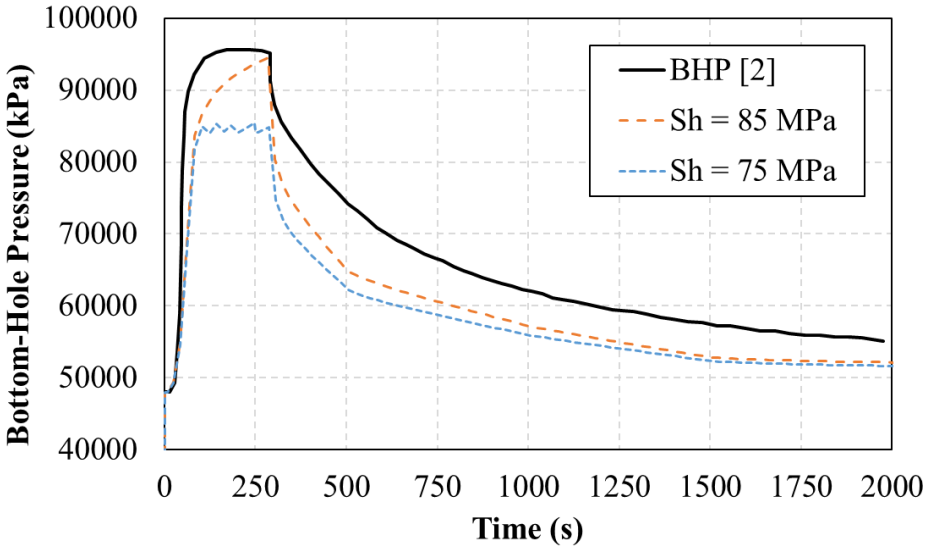

Figure 6 – Bottom-hole pressure considering Sh = 75 MPa and Sh = 85 MPa during the simulation

As can be seen in Figure 6, the minimum horizontal stress plays an important role in the pore pressure curve before and after the closure of the fluid injection rate. However, it is observed that in the final moments after closing, both curves tend to converge.

4.2 Permeability effect

In order to understand the effect of permeability on the DFIT, porous media with different values of permeability (1, 2.5, 5 and 10 mD) are adopted. The numerical simulations are performed considering the minimum horizontal stress σ_h of 85 MPa and the material properties summarized in Table 1 and Table2. Figure 7 shows the bottom-hole pressure curve considering a carbonate reservoir with different permeability values.

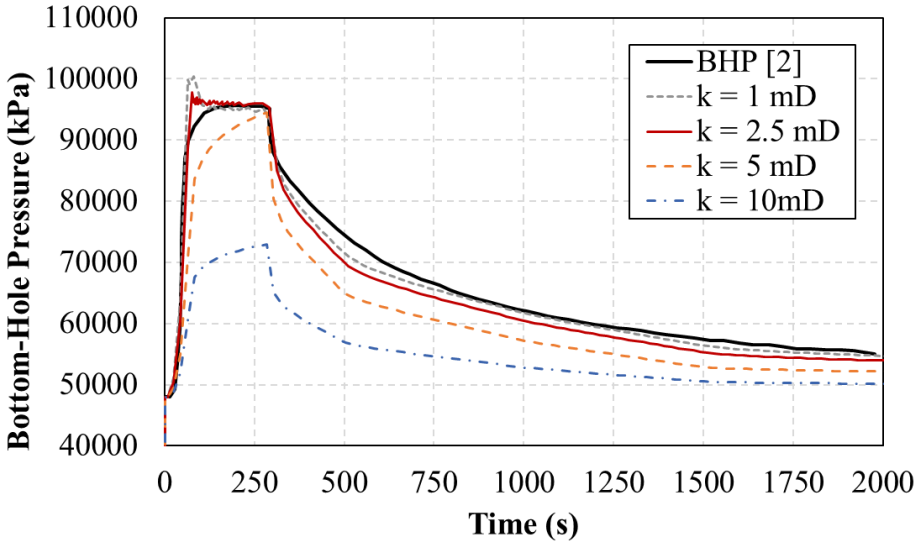

Figure 7 – Bottom-hole pressure considering a porous media with different permeability values.

We can observe that the permeability of rock formation affects all the bottom-hole pressure curve. The Formation Breakdown Pressure (FBP), the peak of the curve, increases as the rock formation permeability decreases. While the Fracture Propagation Pressure (FPP) tends to remain constant because it is mainly defined by the minimum horizontal stresses. However, if the permeability is too high, the injected flow rate may not be sufficient to reach the FBP, and consequently the FPP, thus the fluid will migrate all over the formation without fracture propagation. The numerical results obtained for 1.0 and 2.5 mD show good agreement with the field measured curve. However, the results after the shut-in for 1 mD tends to be closer to the field measured curve. We can conclude that, in the closure stage, a rock formation with a low permeability requires a longer time to dissipate the fluid stored inside the fracture.

4.3 The effect of fracture height

In order to understand the effect of fracture height, the numerical simulations are performed considering three fracture heights (20, 25 and 30m). For all cases, the minimum horizontal stress is 85 MPa, the permeability is 1 mD and material properties detailed in Table 1 and 2 are considered. Figure 8 shows the numerical results considering the effect of fracture height.

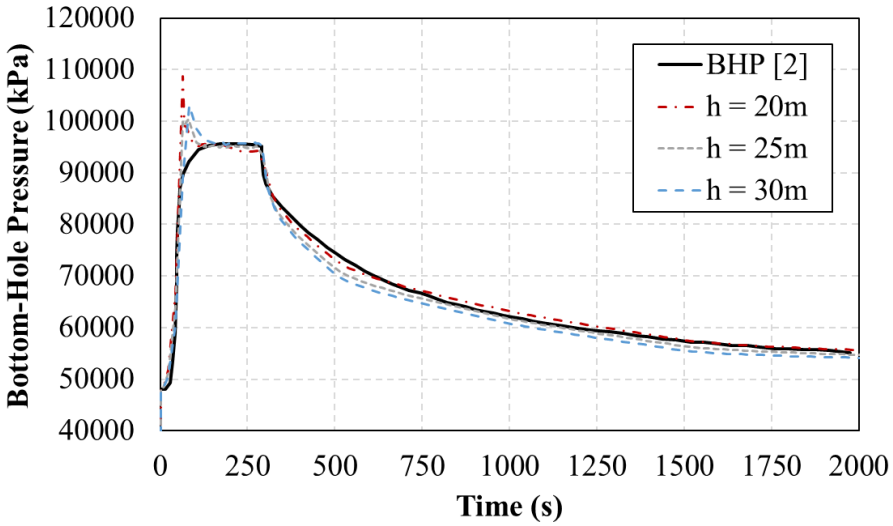

Figure 8 – BHP vs Time for 20 and 25 meters height

As expected, for the same injected fluid rate, a lower fracture height stores a larger fluid volume within the fracture opening, as observed in Figure 9. Consequently, in the closure stage, low fracture height has a small fracture surface requiring a longer time to dissipate the stored fluid. However, the higher the fracture height, the lower FBP is obtained. Although the stress peaks decrease with higher layer thickness, the fracture, propagates faster with lower height. It is also noted that the same minimum horizontal stress impacts different fracture heights, leading to different levels of FPP.

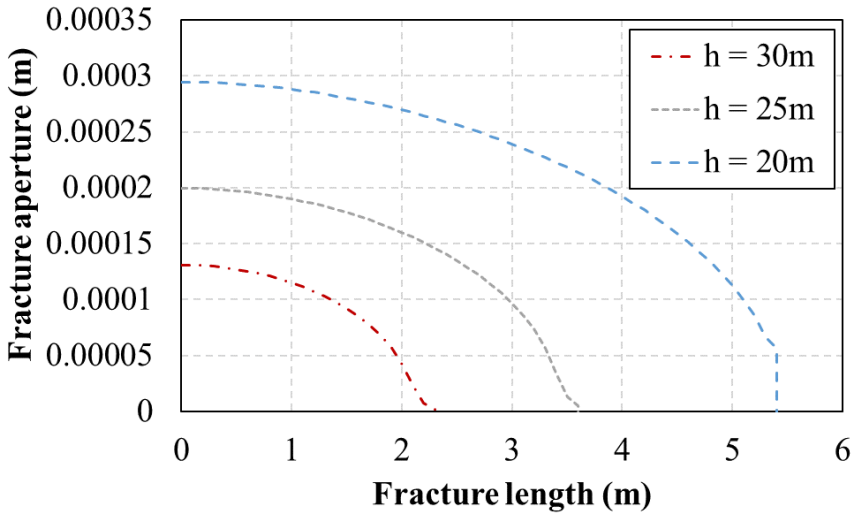

Figure 9 – Fracture aperture vs length at t = 300s

5 Conclusions

This work presents the numerical simulation of DFIT in carbonate reservoirs using fully coupled cohesive elements. The cohesive zone model has proved to be a powerful approach in the finite element method to model hydraulic fracture propagation considering the effect of nonlinear material behavior, permeable porous media and fluid-flow inside the fracture.

The comparison between the numerical results of DFIT and those measured in the field show excellent agreement. The results also show that different parameters affect the bottom-hole pressure curve. Consequently, it is possible to find similar results in the pore pressure curves, for different combinations of parameters.

The effect of in-situ stresses, rock formation permeability and fracture height are also studied. In-situ stresses define the FPP and FBP in the pore pressure curve. While the rock formation permeability affects strongly the bottom-hole pressure curve. Fracture height may be compromised since a planar fracture is estimated. The numerical results show that the fracture height affects the fracture propagation curve and the pore pressure curve at the closure stage. The parametric study presented in this work lays the foundation for the successful numerical calibration of DFIT.

Acknowledgements

The authors gratefully acknowledge support from the Brazilian National Council for Scientific and Technological Development (CNPq).

References

[1] Beltrao RLC, Sombra CL, Lage ACVM, Netto JRF, Henriques CCD. SS: Pre-salt Santos basin - Challenges and New Technologies for the Development of the Pre-salt Cluster, Santos Basin, Brazil. Offshore Technol. Conf., 2009. doi:10.4043/19880-MS.

[2] Azevedo CT, Rosolen M a., Rocha JDH, Neumann LF, Melo RCL. Challenges Faced to Execute Hydraulic Fracturing in Brazilian Pre-Salt. 44th US Rock Mech Symp 2010:1–11.

[3] Wang H, Sharma MM. Determine In-Situ Stress and Characterize Complex Fractures in Naturally Fractured Reservoirs from Diagnostic Fracture Injection Tests. Rock Mech Rock Eng 2019. doi:10.1007/s00603-019-01793-w.

[4] Nolte KG. Fracture Design Considerations Based on Pressure Analysis. SPE Cott. Val. Symp., Society of Petroleum Engineers; 1982. doi:10.2118/10911-MS.

[5] Nguyen DH, Cramer DD. Diagnostic Fracture Injection Testing Tactics in Unconventional Reservoirs, 2013. doi:10.2118/163863-ms.

[6] McClure MW, Blyton CAJ, Jung H, Sharma MM. The Effect of Changing Fracture Compliance on Pressure Transient Behavior During Diagnostic Fracture Injection Tests. SPE Annu. Tech. Conf. Exhib., 2014. doi:10.2118/170956-MS.

[7] Barenblatt GI. Concerning equilibrium cracks forming during brittle fracture. The stability of isolated cracks. Relationships with energetic theories. J Appl Math Mech 1959;23:1273–82. doi:10.1016/0021-8928(59)90130-3.

[8] Dugdale DS. Yielding of steel sheets containing slits. J Mech Phys Solids 1960;8:100–4. doi:10.1016/0022-5096(60)90013-2.

[9] Hillerborg A, Modéer M, Petersson PE. Analysis of crack formation and crack growth in concrete by means of fracture mechanics and finite elements. Cem Concr Res 1976;6:773–81. doi:10.1016/0008-8846(76)90007-7.

[10] Camacho GT, Ortiz M. Computational modelling of impact damage in brittle materials. Int J Solids Struct 1996. doi:10.1016/0020-7683(95)00255-3.

[11] Rueda CJ, Sanchez CM, Roehl D. Hydraulic fracture propagation and its interaction with open and sealed natural fractures. 53rd US Rock Mech Symp 2019.

[12] Rueda Cordero JA, Mejia Sanchez EC, Roehl D, Pereira LC. Hydro-mechanical modeling of hydraulic fracture propagation and its interactions with frictional natural fractures. Comput Geotech 2019;111:290–300. doi:10.1016/j.compgeo.2019.03.020.

[13] Pereira RM de O, Sanchez ECM, Roehl D. A Parametric Study of Mixed-Mode Fracture Propagation in Concrete using XFEM. XXXVIII Iber. Latin-American Congr. Comput. Methods Eng., Florianópolis, SC, Brazil: 2017. doi:10.20906/CPS/CILAMCE2017-0345.

[14] Cruz F, Roehl D, Vargas E do A. An XFEM element to model intersections between hydraulic and natural fractures in porous rocks. Int J Rock Mech Min Sci 2018;112:385–97. doi:10.1016/j.ijrmms.2018.10.001.

[15] Escobar RG, Sanchez EC, Roehl D, Romanel C. Numerical modelling of multiple stage hydraulic fracturing using XFEM. VII Brazilian Symp. Rock Mech. – SBMR 2018, Salvador, Bahia: 2018.

[16] Biot MA. General theory of three-dimensional consolidation. J Appl Phys 1941. doi:10.1063/1.1712886.

[17] Rice JR, Cleary MP. Some basic stress diffusion solutions for fluid-saturated elastic porous media with compressible constituents. Rev Geophys 1976. doi:10.1029/RG014i002p00227.

[18] Zienkiewicx OC, Taylor RL. The Finite Element Method: Solid mechanics Volume 2. 1991. doi:10.1152/jn.00582.2009.

[19] Lewis RW, Schrefler BA. Finite Element Method in the Deformation and Consolidation of Porous Media. 1998. doi:10.1137/1031039.

[20] Papanastasiou P. An efficient algorithm for propagating fluid-driven fractures. Comput Mech 1999. doi:10.1007/s004660050514.

[21] Papanastasiou P. The effective fracture toughness in hydraulic fracturing. Int J Fract 1999. doi:10.1023/A:1018676212444.

[22] Zoback MD. Reservoir Geomechanics. vol. 45. Cambridge: Cambridge University Press; 2007. doi:10.1017/CBO9780511586477.